JACS
JOURNAL OF THE AMERICAN CHEMICAL SOCIETY
Article
pubs.acs.org/JACS

# New Form of an Old Natural Dye: Bay-Annulated Indigo (BAI) as an Excellent Electron Accepting Unit for High Performance Organic Semiconductors

Bo He,[†] Andrew B. Pun,[†] Danylo Zherebetskyy,[‡] Yao Liu,[§] Feng Liu,[‡] Liana M. Klivansky,[†] Alexandra M. McGough,[†] Benjamin A. Zhang,[†] Kelvin Lo,[†,∥] Thomas P. Russell,[§,‡] Linwang Wang,[‡] and Yi Liu*[,†]

[†]The Molecular Foundry and [‡]Materials Sciences Division, Lawrence Berkeley National Laboratory, One Cyclotron Road, Berkeley, California 94720, United States

[§]Department of Polymer Science and Engineering, University of Massachusetts, 120 Governors Drive, Amherst, Massachusetts 01003, United States

[∥]Department of Chemistry, University of California, Berkeley, Berkeley, California 94720, United States

Supporting Information

**ABSTRACT:** A novel electron acceptor was synthesized from one-step functionalization of the readily available indigo dye. The resulting bay-annulated indigo (**BAI**) was utilized for the preparation of a series of novel donor−acceptor small molecules and polymers. As revealed experimentally and by theoretical calculations, substituted **BAIs** have stronger electron accepting characteristics when compared to several premier electron deficient building blocks. As a result, the donor−acceptor materials incorporating **BAI** acceptor possess low-lying LUMO energy levels and small HOMO−LUMO gaps. In situ grazing incidence wide-angle X-ray scattering studies of the thin films of **BAI** donor−acceptor polymers indicated improved crystallinity upon thermal treatment. Field effect transistors based on these polymers show excellent ambipolar transporting behavior, with the hole and electron mobilities reaching 1.5 and 0.41 $cm^2\ V^{-1}\ s^{-1}$, respectively, affirming **BAI** as a potent electron accepting unit for high performance organic electronic materials.

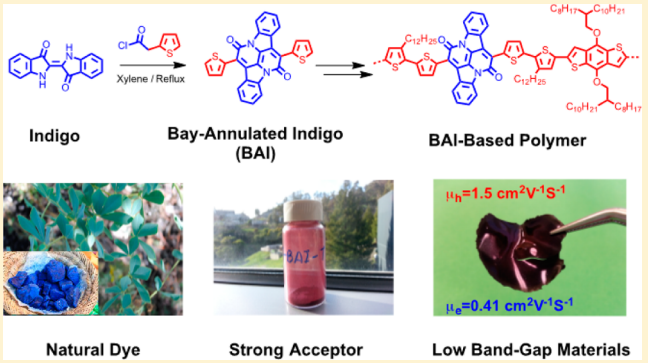


## INTRODUCTION

A major trend in the development of high performance organic semiconductors is reflected by the recent burst of research efforts on low bandgap small molecules and polymers.[1] As a common structural feature of the majority of such materials, alternating electron-rich (donor) and electron-deficient (acceptor) units are linked along the electroactive backbone. The highly modular synthetic protocols, which rely on potent metal catalyzed cross-coupling reactions between electron donors and acceptors, essentially provide access to an unlimited array of functional materials for applications in organic field effect transistors (OFETs)[2] and organic photovoltaics (OPVs).[3] Along the lines of materials discovery, the search for efficient electron donor and acceptor units is one of the most critical steps to better control of key materials parameters, such as electronic energy levels, optical bandgaps and absorptivity, and morphology.[1b,2e] Over the years, several electron acceptors, such as benzothiadiazole (BTD),[4] diketopyrrolopyrrole (DPP),[5] isoindigo (iI),[6] benzobisthiadiazole (BBT)[5f,7] and those based on arylene diimides[8] (Scheme 1a), among others, have become the workhorses in the development of high performance low bandgap materials. Small molecules and polymers incorporating these units have displayed impressive power conversion efficiencies in OPVs and remarkable charge transport mobilities in OFETs.

Some of these acceptors, such as DPP and iI, are based on industrial pigments, which add extra value in terms of materials stability. The centrosymmetric ketopyrrole cores of DPP and isoindigo are, however, not readily available from naturally occurring sources and have to be synthesized in several steps. Indigo, on the other hand, as one of the oldest known dyes, has a similarly appealing symmetric ketopyrrole structure and is an inexpensive pigment material (several US dollars per kilogram) that can be obtained from natural sources or synthetically. Native indigo and other indigoid dyes have received considerable attention for their electron accepting properties and good performance in ambipolar FET transistors.[9] Their

Received: August 26, 2014
Published: September 25, 2014



dx.doi.org/10.1021/ja508807m | J. Am. Chem. Soc. 2014, 136, 15093−15101

**Scheme 1. (a) Structures of Several Commonly Used Electron Acceptors; (b) Illustration of Different Motifs for Functionalizing Indigo**[a]

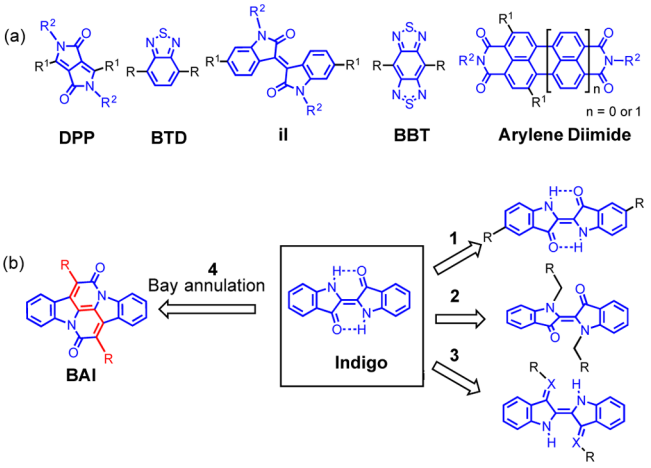


[a]The bonds in red in (b) highlight the conjugation pathway in the **BAI** core.

direct use as semiconducting materials is however restricted, largely due to limited solubility. Considering the isoindigo-based chemistry that has experienced a burst in the past a few years,[6f] it is imperative to build electroactive units directly from the parent indigo to provide more informed search for novel class of functional material systems. Yet a clear chemical pathway to derive practical electroactive units from this high performing dye is still lacking, which warrants detailed experimental and theoretical investigations.

Indigo has a trans-planar molecular structure due to strong intramolecular hydrogen bonding between the two 3-oxindole units that are centrosymmetrically connected by a double bond. Functionalization of indigo can be realized on three positions—one on the two end benzene rings (route 1 in Scheme 1b) and the others on the nitrogen or carbonyl groups at the bay positions of the oxindole units (route 2 and 3 in Scheme 1b). The disadvantage of the former route is that the conjugation does not extend over the central double bond and thus the $\pi$ electron resonance is localized within each oxindole unit. On the other hand, derivatization on the bay positions introduces steric groups that twist the two oxindole units out of plane,[10] unless these units are fixed into a coplanar geometry where both carbonyl groups and N atoms are incorporated into an annulated diketopiperidinopiperidine structure (Scheme 1b, route 4). In addition to reinforced planarity, this annulation also facilitates effective conjugation across the bay—as the part highlighted in red in Scheme 1b—to the substituents. This bay annulated indigo (**BAI**) constitutes the core of the dye *Cibalackrot* that contains two phenyl substituents.[11] Ketone-[12] and N-derivatized indigo[10] have been reported recently, yet little has been explored on the bay annulation chemistry,[13] not to mention the use of **BAI** as electroactive units. Herein we report the synthesis of **BAI** and its use as a new potent electron acceptor. Optical and electrochemical measurements reveal that they have low lying LUMO energies and narrow optical bandgaps. The frontier orbital energies and the optical transitions are verified by detailed computational studies. This electron acceptor is compatible with conventional metal-catalyzed cross-coupling reaction conditions, leading to novel low bandgap donor–acceptor–donor (DAD) triads and donor–acceptor (DA) polymers that possess excellent electronic and optical properties.

## RESULTS AND DISCUSSION

**Materials Synthesis.** Our initial trials targeted at the synthesis of thiophene-flanked **BAI** (Scheme 2) through direct

**Scheme 2. Synthesis of BAI-Based Small Molecules**

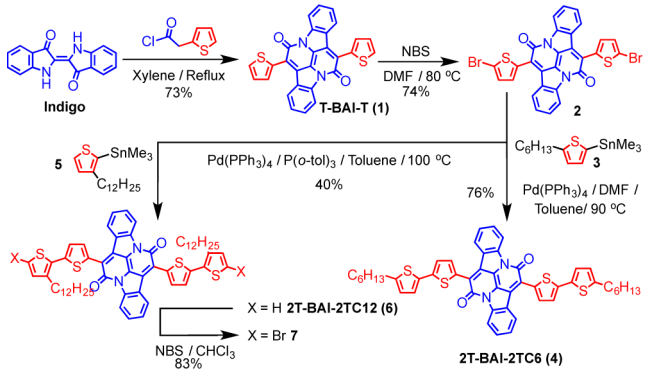


double annulation of the indigo core. Heating a mixture of indigo and 2-thienylacetyl chloride in xylene under reflux gave the purple **T-BAI-T** (**1**) in 73% yield. This double annulation presumably undergoes sequential amidation and intramolecular aldol condensation steps to give the desired product in one pot. Bromination of **1** using *N*-bromosuccinimide (NBS) in DMF yielded dibromide **2** in 74% yield, which underwent Stille coupling with either **3** or **5** to give the DAD type molecules **2T-BAI-2TC6** (**4**) and **2T-BAI-2TC12** (**6**). Further bromination of **6** gave rise to the corresponding dibromide **7**, which polymerized with either the benzodithiophene stannane **8** or carbazole boronic ester **9** to yield DA polymers **P1** or **P2** in 86% and 82% yields, respectively (Scheme 3).

**Scheme 3. Synthesis of Polymers P1 and P2**

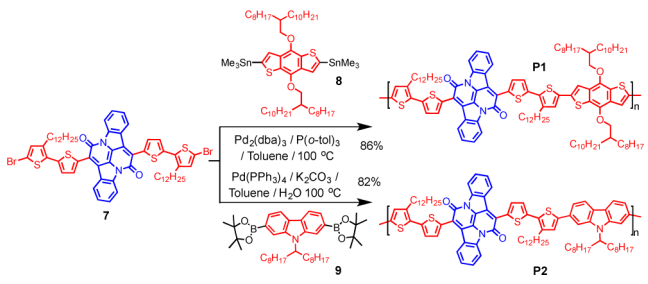


**Optical and Electrochemical Properties.** Optical absorption properties of the **BAI** derivatives were evaluated both in dilute solutions and as thin films (Figure 1), and the relevant data were summarized in Table 1. Solution emission spectra were also included in Figure S1 in Supporting Information. The absorption spectrum of **T-BAI-T** (**1**) displays two absorption bands at 530 and 579 nm, respectively. The former band can be ascribed to the $\pi$–$\pi^*$ transition and the latter attributable to intramolecular charge transfer, which undergoes a bathochromic shift in more polar THF solvent (Figure S2 in Supporting Information) and is characteristic of donor–acceptor systems.[14] The maximum absorption shows a 20–40 nm blue shift with respect to the parent indigo, consistent with indigoids losing intramolecular hydrogen


dx.doi.org/10.1021/ja508807m | J. Am. Chem. Soc. 2014, 136, 15093–15101

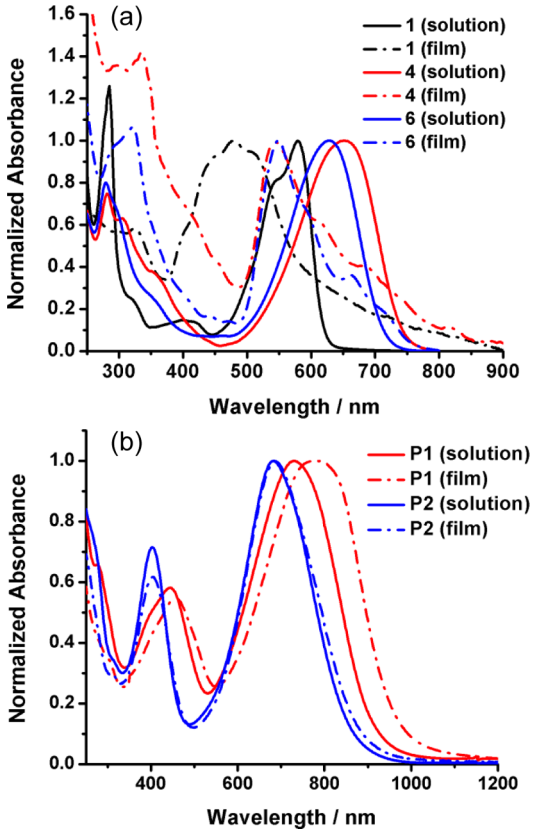


**Figure 1.** UV−vis absorption spectra of the **BAI** (a) small molecules and (b) polymers in $CHCl_3$ solution (solid line) and in thin films (dashed line).

bonding and the "H-chromophore" characteristics.[10] The absorption maxima undergo bathochromic shift to 652 and 629 nm in the cases of **2T-BAI-2TC6** (**4**) and **2T-BAI-2TC12** (**6**), respectively, together with the loss of the fine peak splitting feature. The red shifts are in accordance with extended conjugation involving the extra thiophene units, and the difference between **4** and **6** is attributable to steric induced nonplanarity of the bithiophene units by the 3-alkyl substitution in **6**. The absorption edges at the longest wavelength correspond to optical bandgaps of 1.67 and 1.74 eV for **4** and **6**, respectively. Interestingly, the color of the thin films of **4** and **6** is purple as opposed to the blue color of their solutions, indicating strong H-aggregation in the solid state. This is confirmed by the absorption spectra of thin films of these compounds, which display hypochromic shift of these transitions when compared to their solution spectra (Figure 1a). Such solution-to-thin film spectroscopic shift is reversed (Figure 1b) for the DA polymer **P1**, which has an absorption maximum at 729 nm in solution that shifts bathochromically to 783 nm in thin film. For **P2**, the solution and thin film absorptions peak are nearly overlapping at around 682 nm. The difference for the solution-to-thin film peak shifts between **P1** and **P2** suggests strong interchain interactions in **P1** but less significant in **P2**. The optical bandgaps of these materials are estimated from the onset of absorption of both solution and thin film spectra and listed in Table 1. It should be noted that the bandgap estimation from thin films of small molecules is less accurate due to the strong H-aggregation and ill-defined absorption edges. The strong absorption of **BAI** derivatives in the near IR region is in accordance with the electron withdrawing character of the **BAI** unit. Not surprisingly, **P1** has a smaller bandgap than **P2**, which can be understood by the fact that benzodithiophene (BDT) is a stronger electron donor unit than carbazole and thus gives higher HOMO energy levels.[1a] Since the LUMO energy levels are similar in the two polymers on account of the same **BAI** acceptor unit, the bandgap is smaller in **P1**.

The electrochemical properties of **BAI** compounds were investigated both in solution (Figure 2) and in thin film (Figure S3 in Supporting Information) by cyclic voltammetry using conventional three-electrode setup and ferrocene/ferrocenium ($Fc/Fc^+$) redox couple as the internal reference. Two quasi-reversible one-electron reduction processes are observed for all the **BAI**-based small molecules in solution. The energy levels of the LUMOs of **BAI**-containing compounds are around −3.6

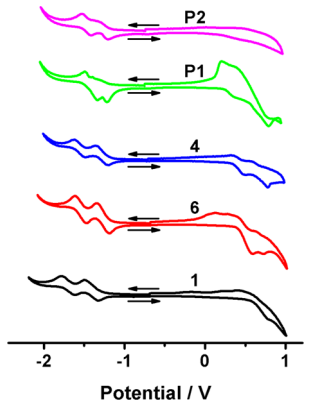


**Figure 2.** Cyclic voltagram of the **BAI** derivatives in $CHCl_3$ solution at a scan rate of 100 mV/s. The potential is referenced to the $Fc/Fc^+$ redox couple.

**Table 1. Summary of Optical and Electrochemical Parameters of BAI derivatives**

| | UV−vis | | | | | | | cyclic voltammetry | | | | |
|---|---|---|---|---|---|---|---|---|---|---|---|---|
| | solution[a] | | | | film | | | | | | | |
| compd | $\lambda_{max}$ (nm) | $\varepsilon_{\lambda max}$ ($M^{-1}$ $cm^{-1}$) | $\lambda_{onset}$ (nm) | $E_g^b$ (eV) | $\lambda_{max}$ (nm) | $\lambda_{onset}$ (nm) | $E_g^c$ (eV) | $E_{1/2}^{Ox,d}$ (V) | $E_{1/2}^{Red,d}$ (V) | $E_{HOMO}$ (eV) | $E_{LUMO}$ (eV) | $E_g^{elec,e}$ (eV) |
| **1** | 579 | 130,200 | 620 | 1.98 | 477 | 703 | 1.76 | 0.51 | −1.41 | −5.38 | −3.53 | 1.85 |
| **4** | 652 | 256,200 | 740 | 1.67 | 545 | 802 | 1.55 | 0.41 | −1.26 | −5.15 | −3.62 | 1.53 |
| **6** | 629 | 320,700 | 712 | 1.74 | 549 | 756 | 1.64 | 0.36 | −1.28 | −5.20 | −3.61 | 1.59 |
| **P1** | 729 | 311,400 | 950 | 1.31 | 783 | 1000 | 1.24 | 0.27 | −1.27 | −4.91 | −3.63 | 1.28 |
| **P2** | 682 | 388,700 | 880 | 1.41 | 685 | 904 | 1.37 | 0.22 | −1.25 | −5.03 | −3.65 | 1.38 |

[a]In $CHCl_3$. [b]Solution optical bandgap. [c]Thin film optical bandgap. [d]Half-wave potentials (vs $Fc/Fc^+$). [e]Solution electrochemical bandgap.


dx.doi.org/10.1021/ja508807m | J. Am. Chem. Soc. 2014, 136, 15093−15101

eV, confirming **BAI**'s excellent electron accepting characteristics. The electrochemical bandgaps in solution match well with the solution optical bandgaps, from which the HOMO energy levels could also be derived (see Table 1).

**Theoretical Modeling of Molecular Orbitals (MOs) and Frontier Orbital Energies (FOEs).** Density functional theory (DFT) calculations were carried out to (1) illustrate the nature of the MOs and the FOEs of **BAI**s, (2) compare their MOs and FOEs against several other commonly used electron acceptors, and (3) understand the influence of donor functionalization on the **BAI** and the corresponding optical transitions. Ground state geometries of the molecules in the solvent were first optimized using 6-31+G(d)[15] basis set. The optimized geometries were then used for characterization of the low-lying excited states relying on time-dependent DFT (TD-DFT) calculations using 6-311++G(d,p) basis set. Since the experimental measurements were done in chloroform solvent, we used continuum solvation model (SMD) based on the quantum mechanical charge density of a solute[16] that shows more reliable results for prediction of the excitation energy.[17] Additionally, calculations using B3LYP/6-311++G(d,p) give reliable results[18] for molecular orbital eigenvalues after linear correlation correction.[19]

Figure 3 and Supporting Information Figure S6 depict the calculated frontier orbitals of several **BAI** derivatives with

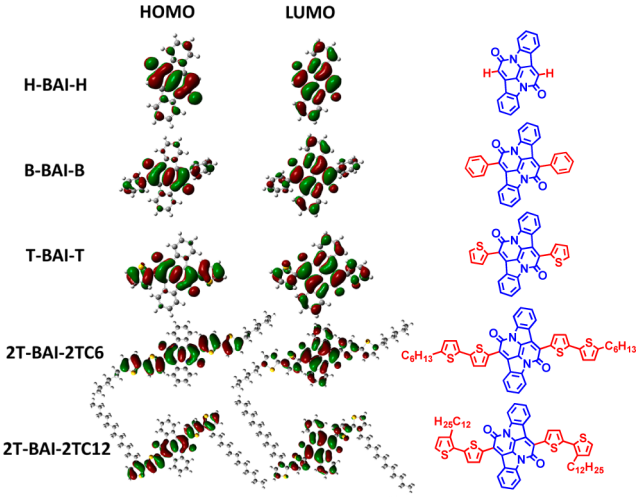


**Figure 3.** Frontier orbitals for the **BAI**s functionalized with different donor units.

different donor groups. The LUMO of the **H-BAI-H** (the unsubstituted **BAI**, not synthesized) is delocalized all over the planar aromatic surface of **BAI**, while HOMO is more localized on diketopiperidopiperidine and both have $\pi^*$-character. Upon functionalization of the **BAI** with benzene or thiophene units, localized HOMOs exhibit significant contribution from the attached donors, with the HOMO spreading over the diketopiperidopiperidine unit and extending to the conjugated donor units but much less so to the two orthogonally arranged benzene rings in the **BAI** core. This clearly confirms our original design highlighted in Scheme 1 that bay annulation indeed facilitates effective conjugation to the attached donors. On the other hand, all LUMOs are highly delocalized over the aromatic surface, including the two annulated benzene rings. The extensive delocalization might account for the low-lying LUMO character of the **BAI** core, while the HOMO is dominated by the conjugation along the orthogonal direction that involves the diketopiperidopiperidine and the thiophene units.

The frontier orbitals and FOEs of the **T-BAI-T** were calculated and compared against **T-DPP-T**, **T-BTD-T**, and **T-iI-T**, all of which are in a similar donor−acceptor−donor fashion and differ mainly by the center acceptor units (Supporting Information Figure S5 and Figure 4). Methyl

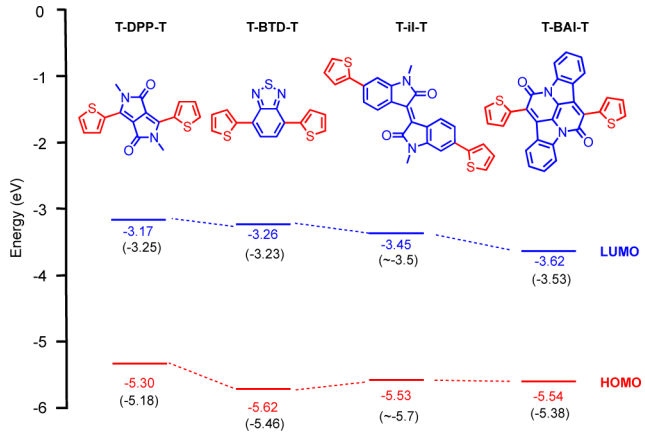


**Figure 4.** Correlation diagram of FOEs of four representative acceptor units. The values in color are calculated FOEs after linear correlation correction, and the values in parentheses are experimental data.

groups are used for N-substituents in the cases of **T-DPP-T** and **T-iI-T** for simplicity. It is noteworthy that the calculated HOMO energies of the molecules are generally in good agreement with experiment, while computed LUMO energies are all overestimated for B3LYP functional (see Table S1 in Supporting Information).[20] Such systematic overestimation has been reported previously and can be adjusted by applying the following linear correlation correction:[19]

$$\varepsilon_{\mathrm{LUMO}}^{\mathrm{exp}} = 1.0729 \cdot \varepsilon_{\mathrm{LUMO}}^{\mathrm{calc}} - 0.181$$

$$\varepsilon_{\mathrm{HOMO}}^{\mathrm{exp}} = 1.001 \cdot \varepsilon_{\mathrm{HOMO}}^{\mathrm{calc}} - 0.050$$

Very good agreement with experimental LUMO energies is obtained after applying the linear correction (Figure 4). The correlation correction is also applied on the HOMO energies, which shows a much smaller effect.

The predicted order of the LUMO energies for the various DAD molecules agrees well with the experimental results. As can be seen from Figure 4, **T-BAI-T** has the lowest LUMO energy, which is about 0.17 eV lower than the second lowest **T-iI-T**. On the other hand, the HOMO is at the similar level to that of **T-iI-T** but significantly lower than that of **T-DPP-T** acceptor. The calculated bandgap is 1.85 eV, also consistent with the experimental optical and electrochemical bandgap measured in solution.

To further understand the effect of functionalization of the **BAI** acceptor by various donor groups, the energy levels of the series of **BAI**-based DAD derivatives are also calculated (Figures 3 and 5). Upon functionalization of the **H-BAI-H** with two flanking benzene units, the HOMO exhibits significant contribution from the benzene rings, while LUMO contains relatively small contribution from the benzene rings. As a result, HOMO of **B-BAI-B** raises its energy by 0.24 eV, while the LUMO level is barely affected compared to these of


dx.doi.org/10.1021/ja508807m | J. Am. Chem. Soc. 2014, 136, 15093−15101

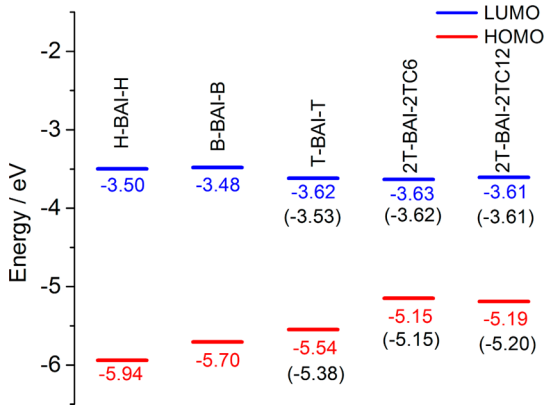


**Figure 5.** Correlation diagram of FOEs of five **BAI** derivatives with different donor units. The values in color are calculated FOEs after linear correlation correction, and the values in parentheses are experimental data.

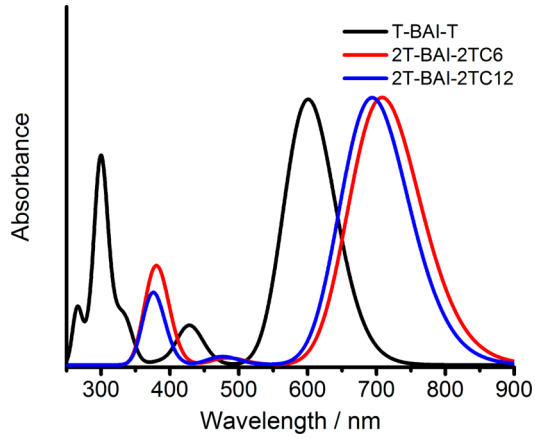


**Figure 6.** TD-DFT calculated electronic absorption spectra of the **BAI** derivatives.

the **H-BAI-H**. Thiophene functionalization of **BAI** also results in extended delocalization of HOMO. This delocalization is even more significant than in **B-BAI-B**, resulting in an increase of the HOMO level by 0.4 eV in **T-BAI-T**. LUMO also has some contribution from the thiophene units, which leads to greater overlap with HOMO and subsequently stronger HOMO−LUMO columbic interaction. Consequently, the LUMO is further stabilized by 0.14 eV when compare to benzene substituted **B-BAI-B**. Addition of another thiophene ring to each side of **T-BAI-T** results in even more delocalized HOMO, further raising its energy by around 0.4 eV, while LUMO is barely affected. However, there is a slight variation between differently functionalized **2T-BAI-2TC6** (**4**) and **2T-BAI-2TC12** (**6**). Thiophene−thiophene dihedral angles for **4** and **6** are 16° and 21°, respectively. This difference implies better conjugation between thiophene groups for **4**, resulting in higher HOMO and slightly lower LUMO. Indeed, this is consistent with previous investigations of the impact of the dihedral angles on HOMO and LUMO energies,[21] which show that increasing the dihedral angle lowers the HOMO and raises LUMO.

The effects of the donor functionalization on the frontier orbitals and their energy levels also account for the differences in their electronic absorption spectra, as calculated using time-dependent DFT (TD-DFT). Since **T-BAI-T** is smaller than **2T-BAI-2TC6** and **2T-BAI-2TC12**, we calculated the first 20 singlet excitations for the former and 10 singlet excitations for the others; thus, only absorption bands above 350 nm are calculated for the latter two bigger molecules. Qualitatively, the calculated (Figure 6) and experimental (Figure 4) spectra are in good agreement, including the relative positions and number of adsorption bands, except that the experimental spectrum of **T-BAI-T** has an additional shoulder that is attributed to the intramolecular charge transfer.[14] The lowest energy excitation is attributed to HOMO−LUMO transition in all molecules (Table S2 in Supporting Information). It should be noted that there is no HOMO → LUMO + 1 intramolecular charge transfer transition. Though inclusion of the triplet excitations results in appearance of HOMO → LUMO + 1 transition mixed with HOMO − 1 → LUMO transition at 2.01 eV (616 nm), oscillator strength of this excitation is 0 (see Table S2 in Supporting Information). This can explain why the computed result does not show the charge transfer shoulder in the **T-BAI-T** molecule. In reality, this transition can be caused by lowered molecular symmetry, phonon-assisted processes, or other more complicated processes which are not accounted for during the calculations.

**Charge Transport and Morphological Studies of Polymers.** **BAI**'s strong electron accepting properties make their derivatives great candidates for n-type or ambipolar electronic materials, which are of particular interests for the application in integrated circuits.[22] We thus investigated the charge carrier transport properties of the two **BAI**-containing polymers **P1** and **P2** in OFET devices. Bottom-gate/bottom-contact (BG/BC) devices were fabricated by spin coating polymer solutions in $CHCl_3$ onto silicon substrates (with a 300 nm-thick thermally grown oxide layer) that were predeposited with octadecyltrichlorosilane and Au/Cr source and drain electrodes. All devices were fabricated and annealed at 160 °C in gloveboxes. Both **P1** and **P2** show ambipolar behavior when the OFET devices were tested under high vacuum ($1 \times 10^{-6}$ mbar). For **P1**, the maximum hole and electron mobilities reach 1.5 and 0.41 $cm^2\ V^{-1}\ s^{-1}$, respectively, and for **P2**, the maximum hole and electron mobilities are 0.14 and 0.09 $cm^2\ V^{-1}\ s^{-1}$, respectively (Table 2 and Figure 7). When measured in air, the corresponding devices show only unipolar hole transporting behavior with comparable hole mobilities (Table 2 and Supporting Information Figure S7). The lack of electron transporting in the air is ascribed to the trapping of electrons by $H_2O$ or $O_2$.[2e,23] Nevertheless, the ambipolar transporting properties correlate well with the electron accepting properties of **BAI** unit. Further lowering of the LUMO of **BAI**-based materials below −4.0 eV should increase the air stability and is a subject of future study.[2e]

Grazing incident wide-angle X-ray scattering (GIWAXS) measurements were conducted to probe the molecular packing within the spin-coated films of **P1** and **P2**. For the as-spun thin film of **P1**, a strong (100) scattering peak with a spacing of 2.24 nm is oriented in the out-of-plane (OOP) direction with a broad angular distribution, indicating slight preferential orientation of the polymer chains on the substrate. A second-order diffraction peak is also observed in the OOP direction, confirming the edge-on orientation. An additional azimuthally independent broad reflection is seen at ~1.54 $A^{-1}$, which arises from the average chain separation distance of the amorphous part of the polymer. When the sample is thermally annealed at 250 °C for 10 min and cooled back to room temperature, the structural order of the film is greatly improved. Higher order


dx.doi.org/10.1021/ja508807m | J. Am. Chem. Soc. 2014, 136, 15093−15101

**Table 2. Summary of OFET Characteristics of P1 and P2**

| compd | $\mu_{max,h}/\mu_{max,e}$ [c] | $\mu_{aver,h}/\mu_{ave,e}$ [d] | $V_{th,h}/V_{th,e}$ [e] | $I_{On}/I_{Off}$ (h/e) [f] |
|---|---|---|---|---|
| **P1**[a] | 1.5/0.41 | 1.4/0.36 | −5.7−7.2/50−53 | $3 \times 10^3$−$2 \times 10^4$/$3 \times 10^1$−$3 \times 10^2$ |
| **P1**[b] | 1.7/- | 1.3/- | 20−22/-- | $3 \times 10^3$−$5 \times 10^4$/- |
| **P2**[a] | 0.14/0.09 | 0.12/0.07 | −19−22/34−38 | $2 \times 10^3$−$5 \times 10^3$/$5 \times 10^2$−$6 \times 10^2$ |
| **P2**[b] | 0.36/- | 0.32/- | 20−23/- | $1 \times 10^3$−$2 \times 10^4$/-- |

[a]Measured in vacuum. [b]Measured in air. [c]Maximum hole and electron mobilities. [d]Average hole and electron mobilities. [e]Threshold voltages for hole and electron transporting region. [f]On/off ratio for hole and electron transporting region.

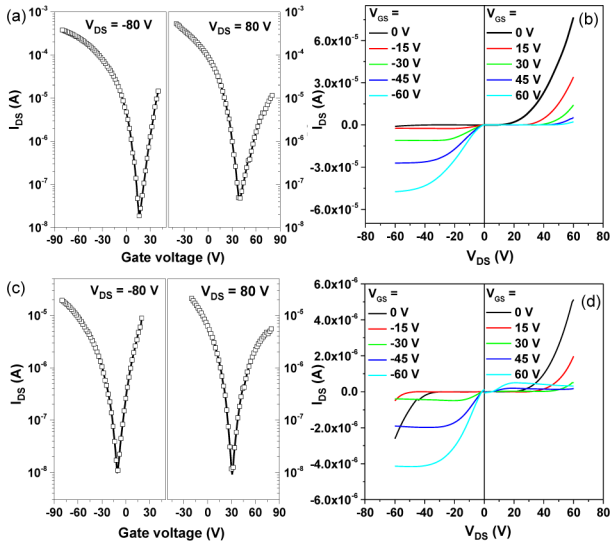


**Figure 7.** (a) Output and (b) transfer characteristics of **P1**-based OFETs; (c) output and (d) transfer characteristics of **P2**-based OFETs. The devices are annealed at 160 °C before being tested in vacuum.

(100) reflections become more pronounced, accompanied by significant reduction in the intensity of the amorphous halo, indicating a largely enhanced crystallinity of the film. The angular distribution of the (100) peak is much narrower and more focused in the direction normal to the film surface and the (010) reflection, characteristic of the $\pi-\pi$ stacking (3.83 Å) being clearly evident in the plane of the film, in keeping with an edge-on packing. **P2** polymer thin film shows a quite different morphology. A (100) reflection, oriented normal to the film surface, with a characteristic distance of ∼1.46 nm, much less than that of **P1**, is seen, indicating that the side chains of the polymer are highly frustrated. It should be noted that this reflection and two higher order reflections are also observed in the in-plane direction, indicating that **P2** chains take a mixed edge-on and face-on orientation. A diffuse halo with a slight intensification in OOP direction is seen at 1.52 $A^{-1}$, corresponding to a distance of 4.13 Å. After annealing the **P2** thin film at 250 °C for 10 min, a hexagonal packing emerges with a characteristic distance of 22.4 Å. The amorphous halo is still present, though weaker. It is apparent that altering the BDT copolymerization unit to carbazole leads to drastic change in packing, which is expected from their chemical structure origin. **BAI-BDT** copolymer **P1** shows a more planner chain conformation, as seen from the small dihedral angle between the two copolymerization units. Thermal annealing imparts mobility to the polymer chains, promoting an intermolecular packing into ordered structures, with $\pi-\pi$ stacking retained in in-plane direction. Such packing facilitates lateral charge transport in the thin film transistors, leading to high mobility. Incorporation of carbazole unit leads to twisting and larger dihedral angle between the two copolymerization units. The long branched side chains on carbazole unit further keep the backbone $\pi$ surfaces from approaching each other, consequently no obvious $\pi-\pi$ stacking signal is seen in GIWAXS. In thermally annealed samples, the hexagonal packing is a direct consequence of conformational complexity of **P2** polymer chain,[24] which should be viewed as a rod since thermal energy activates free rotation of the copolymerized repeating units. $\pi-\pi$ Interactions are, however, strongly restricted, and, thus, the formation of lamellae packing is disfavored. The observed difference in interchain $\pi-\pi$ stacking in the thin films of **P1** and **P2** correlates very well with the UV−vis spectra absorption shifts (Figure 1b). For **P1**, there is a significant red shift (54 nm) of the lowest energy transition from solution to thin film, while in the case of **P2**, there is barely any shift. The hexagonal packing in **P2** is not ideal for charge transport from the perspective of $\pi-\pi$ stacking assisted hopping mechanism. Nevertheless, moderate mobilities are recorded, which are higher than the state-of-the art $\pi-\pi$ hopping transport model of PBTTT[25] and P3HT.[24] This result suggests that other charge transporting pathways, such as in-chain transport, and tight chain hoping might be contributing to the mobility.[26] A more detailed study of structural evolution by GIWAXS at different temperatures was carried out under *in situ* thermal annealing, where thin film samples were mounted on a heating stage inside a helium box. A ramping rate of 10 °C/min was used in the heating cycle and natural cooling was used for the cool-down process. For **P1** samples, polymer chains start to become ordered at 100 °C (Figure 8). When the temperature is raised

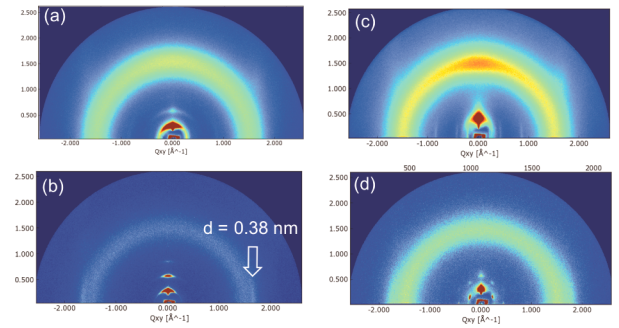


**Figure 8.** GIWAXS of spun-cast thin films of (a and b) **P1** and (c and d) **P2**; (a and c) as cast films; (b and d) annealed films.

to 150 °C, the growth of (100) becomes obvious while the azimuthal distribution of this peak remains quite broad (Figure 9). Further increasing the temperature to 200 °C induces higher order diffraction peaks, meanwhile $\pi-\pi$ stacking peak also becomes more obvious. At 250 °C, the azimuthal distrubtion of (100) peak is significantly narrowed, indicating that in this temperature range crystals reorganize into edge-on


dx.doi.org/10.1021/ja508807m | J. Am. Chem. Soc. 2014, 136, 15093−15101

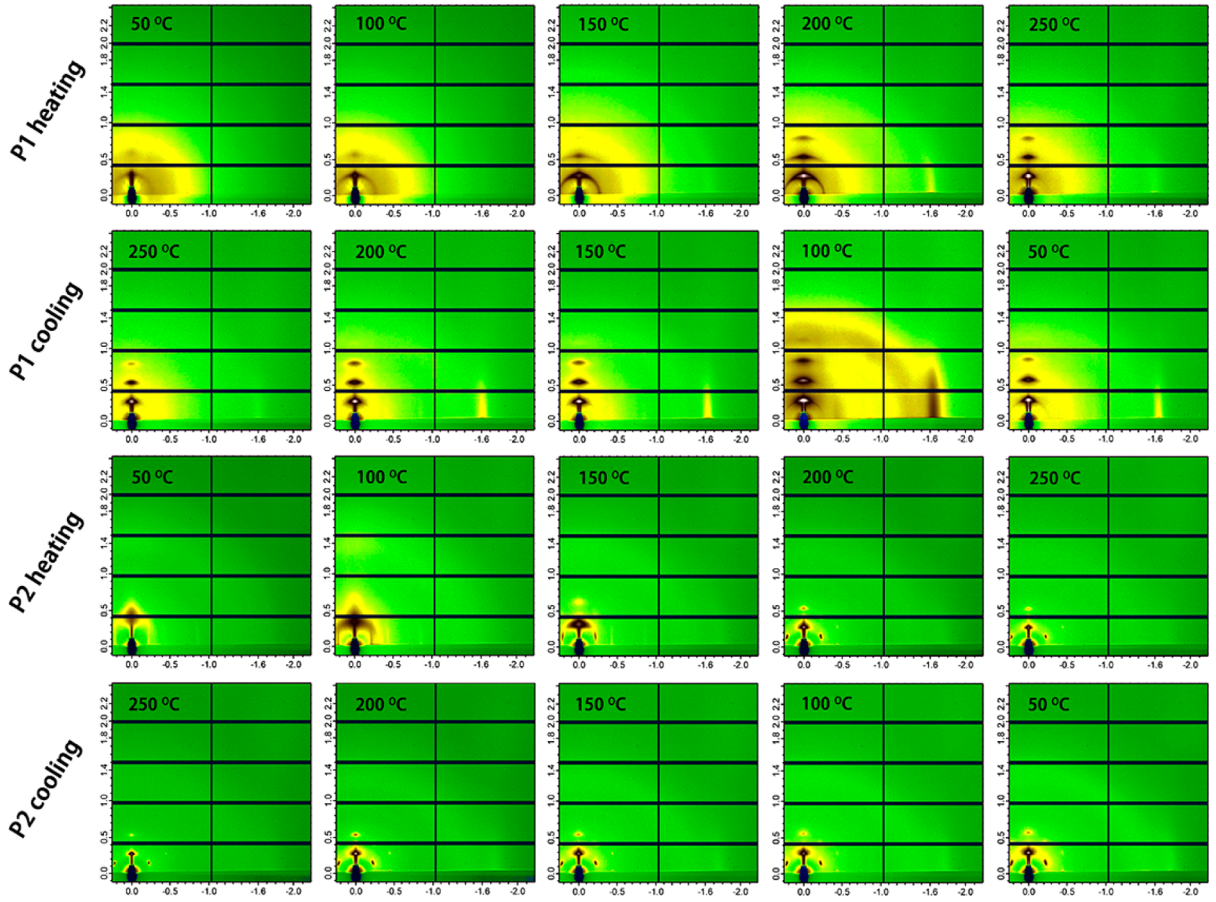


**Figure 9.** GIWAXS patterns of thin films of **P1** and **P2** taken during *in situ* heating and cooling cycles.

orientation, presumably due to the chain-substrate interactions. During the subsequent cooling process, this edge-on orientation is retained. For **P2** samples, evident ordering process emerges above 100 °C, and the packing transforms to a hexagonal structure from above 150 °C. At temperatures above 200 °C, a fairly strong hexagonal lattice is observed in the GIWAXS images. During subsequent cooling this packing structure is also retained.

Atomic force microscopic (AFM) images of both unannealed polymer films revealed (Figure 10) the formation of fiber-like intercalating networks. Consistent with thermally induced molecular reorganization and changes of molecular packing within the films, crystallite domain size and the roughness increased slightly after annealing in each case. It is noteworthy that void spaces were present in both **P1** and **P2** thin films, which are not desirable for charge transport as such grain boundaries can cause an energy barrier and limit charge carrier mobilities in thin films.[27] As demonstrated by Pei and others,[28] modification of the polymers by altering the side chain structures is an effective way to enhance molecular order and packing within the thin film. Given that no significant efforts have been made to optimize the thin films and the device performances, it is reasonable to expect that more efficient carrier transport can be realized in **BAI**-based materials with further side chain engineering.

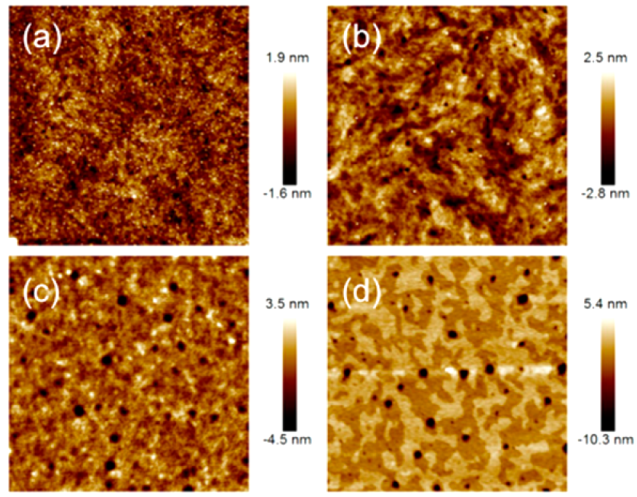


**Figure 10.** AFM images (2 $\mu$m × 2 $\mu$m) of (a and b) **P1**, and (c and d) **P2**; (a and c) as cast films; (b and d) annealed films.

## ■ CONCLUSIONS

In summary, we have designed and synthesized a new electron acceptor unit that is based on the cheap and one of the oldest naturally occurring indigo dye. The synthesis of **BAI** is realized by a one-pot reaction that involves double annulation steps to give a new annulated diketopiperidinopiperidine core. The derivatization on the indigo ensures extension of the $\pi$-conjugation without disturbing the planarity of indigo, resulting in novel electron acceptors that have deeper LUMO energy level than reported imide-based acceptors such as isoindigo and DPP derivatives. Detailed theoretical calculations have been carried out to understand the frontier orbitals and energies, as


dx.doi.org/10.1021/ja508807m | J. Am. Chem. Soc. 2014, 136, 15093−15101

well as electronic transitions of **BAI** derivatives. The versatility of the **BAI** acceptor has been demonstrated by its facile incorporation into donor−acceptor small molecules and low bandgap polymers through conventional metal-catalyzed cross-coupling reactions. The preferred formation of lamellar or hexagonal packing in thin films of the two **BAI** polymers upon thermal annealing, as revealed by *in situ* GIWAXS experiments, attests to different interchain interactions and well-behaved self-assembly processes that are also dependent on the conformation of the conjugated backbone. The OFETs based on solution processed thin films of both **BAI** polymers have shown ambipolar transport properties, with high hole and electron mobilities reaching 1.5 and 0.41 $cm^2\ V^{-1}\ s^{-1}$, respectively. With the added benefits of easy access to cheap starting material and the straightforward chemistry, this **BAI** acceptor is poised as a versatile electron deficient building block that is readily available for the discovery of new series of high performance optoelectronic materials.

## ■ ASSOCIATED CONTENT

### Ⓢ Supporting Information

Experimental methods; synthesis and characterization details; Frontier molecular orbitals and energies; OFET device characteristics. This material is available free of charge via the Internet at http://pubs.acs.org.

## ■ AUTHOR INFORMATION


### Corresponding Author

yliu@lbl.gov


### Notes

The authors declare no competing financial interest.

## ■ ACKNOWLEDGMENTS

This work was supported by Self-Assembly of Organic/Inorganic Nanocomposite Materials program, and was performed at the Molecular Foundry, both supported by the Office of Science, Office of Basic Energy Sciences, of the U.S. Department of Energy under Contract No. DE-AC02-05CH11231. The X-ray scattering experiments were conducted at the Advanced Light Source (ALS), Lawrence Berkeley National Laboratory, and Stanford Synchrotron Radiation Lightsource (SSRL). A.B.P. acknowledges the DOE SULI internship program. We thank Dr. Chenhui Zhu and Dr. Alexander Hexemer at BL7.3.3 of ALS and David Hanifi at Stanford University for help with X-ray scattering experiments. This work used the resource of National Energy Research Scientific Computing Center (NERSC) which is founded by the U.S. Department of Energy.

## ■ REFERENCES


(1) (a) Zhang, Z. G.; Wang, J. *J. Mater. Chem.* **2012**, *22*, 4178−4187. (b) Takimiya, K.; Osaka, I.; Nakano, M. *Chem. Mater.* **2013**, *26*, 587−593. (c) Beaujuge, P. M.; Fréchet, J. M. J. *J. Am. Chem. Soc.* **2011**, *133*, 20009−20029.

(2) (a) Wang, C.; Dong, H.; Hu, W.; Liu, Y.; Zhu, D. *Chem. Rev.* **2011**, *112*, 2208−2267. (b) Mei, J.; Diao, Y.; Appleton, A. L.; Fang, L.; Bao, Z. *J. Am. Chem. Soc.* **2013**, *135*, 6724−6746. (c) Dong, H.; Fu, X.; Liu, J.; Wang, Z.; Hu, W. *Adv. Mater.* **2013**, *25*, 6158−6183. (d) Li, H.; Kim, F. S.; Ren, G.; Jenekhe, S. A. *J. Am. Chem. Soc.* **2013**, *135*, 14920−14923. (e) Zhao, Y.; Guo, Y.; Liu, Y. *Adv. Mater.* **2013**, *25*, 5372−5391. (f) Cai, Z.; Luo, H.; Qi, P.; Wang, J.; Zhang, G.; Liu, Z.; Zhang, D. *Macromolecules* **2014**, *47*, 2899−2906. (g) Takeda, Y.; Andrew, T. L.; Lobez, J. M.; Mork, A. J.; Swager, T. M. *Angew. Chem., Int. Ed.* **2012**, *51*, 9042−9046. (h) Lei, T.; Xia, X.; Wang, J.-Y.; Liu, C.-J.; Pei, J. *J. Am. Chem. Soc.* **2014**, *136*, 2135−2141.

(3) (a) Cheng, Y.-J.; Yang, S.-H.; Hsu, C.-S. *Chem. Rev.* **2009**, *109*, 5868−5923. (b) Kularatne, R. S.; Magurudeniya, H. D.; Sista, P.; Biewer, M. C.; Stefan, M. C. *J. Polym. Sci., Part A: Polym. Chem.* **2013**, *51*, 743−768. (c) Thompson, B. C.; Frechet, J. M. J. *Angew. Chem., Int. Ed.* **2008**, *47*, 58−77. (d) Li, Y.; Yao, K.; Yip, H.-L.; Ding, F.-Z.; Xu, Y.-X.; Li, X.; Chen, Y.; Jen, A. K. Y. *Adv. Funct. Mater.* **2014**, *24*, 3631−3638. (e) Warnan, J.; Cabanetos, C.; Bude, R.; El Labban, A.; Li, L.; Beaujuge, P. M. *Chem. Mater.* **2014**, *26*, 2829−2835. (f) Huang, Y.; Kramer, E. J.; Heeger, A. J.; Bazan, G. C. *Chem. Rev.* **2014**, *114*, 7006−7043. (g) Cabanetos, C.; El Labban, A.; Bartelt, J. A.; Douglas, J. D.; Mateker, W. R.; Fréchet, J. M. J.; McGehee, M. D.; Beaujuge, P. M. *J. Am. Chem. Soc.* **2013**, *135*, 4656−4659.

(4) (a) Tsao, H. N.; Cho, D. M.; Park, I.; Hansen, M. R.; Mavrinskiy, A.; Yoon, D. Y.; Graf, R.; Pisula, W.; Spiess, H. W.; Müllen, K. *J. Am. Chem. Soc.* **2011**, *133*, 2605−2612. (b) Tseng, H.-R.; Ying, L.; Hsu, B. B. Y.; Perez, L. A.; Takacs, C. J.; Bazan, G. C.; Heeger, A. J. *Nano Lett.* **2012**, *12*, 6353−6357. (c) Beaujuge, P. M.; Tsao, H. N.; Hansen, M. R.; Amb, C. M.; Risko, C.; Subbiah, J.; Choudhury, K. R.; Mavrinskiy, A.; Pisula, W.; Brédas, J.-L.; So, F.; Müllen, K.; Reynolds, J. R. *J. Am. Chem. Soc.* **2012**, *134*, 8944−8957.

(5) (a) Qu, S.; Tian, H. *Chem. Commun.* **2012**, *48*, 3039−3051. (b) Nielsen, C. B.; Turbiez, M.; McCulloch, I. *Adv. Mater.* **2013**, *25*, 1859−1880. (c) Kanimozhi, C.; Yaacobi-Gross, N.; Chou, K. W.; Amassian, A.; Anthopoulos, T. D.; Patil, S. *J. Am. Chem. Soc.* **2012**, *134*, 16532−16535. (d) Bronstein, H.; Chen, Z.; Ashraf, R. S.; Zhang, W.; Du, J.; Durrant, J. R.; Shakya Tuladhar, P.; Song, K.; Watkins, S. E.; Geerts, Y.; Wienk, M. M.; Janssen, R. A. J.; Anthopoulos, T.; Sirringhaus, H.; Heeney, M.; McCulloch, I. *J. Am. Chem. Soc.* **2011**, *133*, 3272−3275. (e) Li, W.; Roelofs, W. S. C.; Wienk, M. M.; Janssen, R. A. J. *J. Am. Chem. Soc.* **2012**, *134*, 13787−13795. (f) Yuen, J. D.; Fan, J.; Seifter, J.; Lim, B.; Hufschmid, R.; Heeger, A. J.; Wudl, F. *J. Am. Chem. Soc.* **2011**, *133*, 20799−20807. (g) Loser, S.; Bruns, C. J.; Miyauchi, H.; Ortiz, R. P.; Facchetti, A.; Stupp, S. I.; Marks, T. J. *J. Am. Chem. Soc.* **2011**, *133*, 8142−8145.

(6) (a) Mei, J.; Kim, D. H.; Ayzner, A. L.; Toney, M. F.; Bao, Z. *J. Am. Chem. Soc.* **2011**, *133*, 20130−20133. (b) Lei, T.; Cao, Y.; Fan, Y.; Liu, C.-J.; Yuan, S.-C.; Pei, J. *J. Am. Chem. Soc.* **2011**, *133*, 6099−6101. (c) Lei, T.; Cao, Y.; Zhou, X.; Peng, Y.; Bian, J.; Pei, J. *Chem. Mater.* **2012**, *24*, 1762−1770. (d) Wang, E.; Ma, Z.; Zhang, Z.; Vandewal, K.; Henriksson, P.; Inganäs, O.; Zhang, F.; Andersson, M. R. *J. Am. Chem. Soc.* **2011**, *133*, 14244−14247. (e) Mei, J. G.; Graham, K. R.; Stalder, R.; Reynolds, J. R. *Org. Lett.* **2010**, *12*, 660−663. (f) Stalder, R.; Mei, J.; Graham, K. R.; Estrada, L. A.; Reynolds, J. R. *Chem. Mater.* **2013**, *26*, 664−678.

(7) Fan, J.; Yuen, J. D.; Cui, W.; Seifter, J.; Mohebbi, A. R.; Wang, M.; Zhou, H.; Heeger, A.; Wudl, F. *Adv. Mater.* **2012**, *24*, 6164−6168.

(8) (a) Zhan, X.; Facchetti, A.; Barlow, S.; Marks, T. J.; Ratner, M. A.; Wasielewski, M. R.; Marder, S. R. *Adv. Mater.* **2011**, *23*, 268−284. (b) Yan, H.; Chen, Z.; Zheng, Y.; Newman, C.; Quinn, J. R.; Dotz, F.; Kastler, M.; Facchetti, A. *Nature* **2009**, *457*, 679−686. (c) Schmidt, R.; Ling, M. M.; Oh, J. H.; Winkler, M.; Könemann, M.; Bao, Z.; Würthner, F. *Adv. Mater.* **2007**, *19*, 3692−3695. (d) Lv, A.; Puniredd, S. R.; Zhang, J.; Li, Z.; Zhu, H.; Jiang, W.; Dong, H.; He, Y.; Jiang, L.; Li, Y.; Pisula, W.; Meng, Q.; Hu, W.; Wang, Z. *Adv. Mater.* **2012**, *24*, 2626−2630. (e) Zhan, X.; Tan, Z. a.; Domercq, B.; An, Z.; Zhang, X.; Barlow, S.; Li, Y.; Zhu, D.; Kippelen, B.; Marder, S. R. *J. Am. Chem. Soc.* **2007**, *129*, 7246−7247. (f) Fukutomi, Y.; Nakano, M.; Hu, J.-Y.; Osaka, I.; Takimiya, K. *J. Am. Chem. Soc.* **2013**, *135*, 11445−11448. (g) Zhao, J.; Wong, J. I.; Gao, J.; Li, G.; Xing, G.; Zhang, H.; Sum, T. C.; Yang, H. Y.; Zhao, Y.; Ake Kjelleberg, S. L.; Huang, W.; Joachim Loo, S. C.; Zhang, Q. *RSC Adv.* **2014**, *4*, 17822−17831.

(9) (a) Glowacki, E. D.; Voss, G.; Sariciftci, N. S. *Adv. Mater.* **2013**, *25*, 6783−6800. (b) Głowacki, E. D.; Voss, G.; Leonat, L.; Irimia-Vladu, M.; Bauer, S.; Sariciftci, N. S. *Isr. J. Chem.* **2012**, *52*, 540−551. (c) Irimia-Vladu, M.; Glowacki, E. D.; Troshin, P. A.; Schwabegger, G.; Leonat, L.; Susarova, D. K.; Krystal, O.; Ullah, M.; Kanbur, Y.; Bodea, M. A.; Razumov, V. F.; Sitter, H.; Bauer, S.; Sariciftci, N. S. *Adv. Mater.*

**2012**, *24*, 375−380. (d) Robb, M. J.; Ku, S.-Y.; Brunetti, F. G.; Hawker, C. J. *J. Polym. Sci., Part A: Polym. Chem.* **2013**, *51*, 1263−1271.
(10) Glowacki, E. D.; Voss, G.; Demirak, K.; Havlicek, M.; Sunger, N.; Okur, A. C.; Monkowius, U.; Gasiorowski, J.; Leonat, L.; Sariciftci, N. S. *Chem. Commun.* **2013**, *49*, 6063−6065.
(11) Seixas de Melo, J.; Rondão, R.; Burrows, H. D.; Melo, M. J.; Navaratnam, S.; Edge, R.; Voss, G. *J. Phys. Chem. A* **2006**, *110*, 13653−13661.
(12) Nawn, G.; Oakley, S. R.; Majewski, M. B.; McDonald, R.; Patrick, B. O.; Hicks, R. G. *Chem. Sci.* **2013**, *4*, 612−621.
(13) (a) Engi, G. *Angew. Chem.* **1914**, *27*, 144−148. (b) Posner, T.; Kemper, W. *Ber. Dtsch. Chem. Ges. A/B* **1924**, *57*, 1311−1315.
(14) Stalder, R.; Mei, J. G.; Reynolds, J. R. *Macromolecules* **2010**, *43*, 8348−8352.
(15) (a) Binkley, J. S.; Pople, J. A.; Hehre, W. J. *J. Am. Chem. Soc.* **1980**, *102*, 939−947. (b) Krishnan, R.; Binkley, J. S.; Seeger, R.; Pople, J. A. *J. Chem. Phys.* **1980**, *72*, 650−654.
(16) Marenich, A. V.; Cramer, C. J.; Truhlar, D. G. *J. Phys. Chem. B* **2009**, *113*, 6378−6396.
(17) Fleming, S.; Mills, A.; Tuttle, T. *Beilstein J. Org. Chem.* **2011**, *7*, 432−441.
(18) Kaur, I.; Jia, W.; Kopreski, R. P.; Selvarasah, S.; Dokmeci, M. R.; Pramanik, C.; McGruer, N. E.; Miller, G. P. *J. Am. Chem. Soc.* **2008**, *130*, 16274−16286.
(19) Zhan, C.-G.; Nichols, J. A.; Dixon, D. A. *J. Phys. Chem. A* **2003**, *107*, 4184−4195.
(20) Tao, Y.; Yang, C.; Qin, J. *Chem. Soc. Rev.* **2011**, *40*, 2943−2970.
(21) Brownell, L. V.; Robins, K. A.; Jeong, Y.; Lee, Y.; Lee, D.-C. *J. Phys. Chem. C* **2013**, *117*, 25236−25247.
(22) Zaumseil, J.; Sirringhaus, H. *Chem. Rev.* **2007**, *107*, 1296−1323.
(23) Brown, A. R.; Jarrett, C. P.; de Leeuw, D. M.; Matters, M. *Synth. Met.* **1997**, *88*, 37−55.
(24) Ko, S.; Hoke, E. T.; Pandey, L.; Hong, S.; Mondal, R.; Risko, C.; Yi, Y.; Noriega, R.; McGehee, M. D.; Brédas, J.-L.; Salleo, A.; Bao, Z. *J. Am. Chem. Soc.* **2012**, *134*, 5222−5232.
(25) McCulloch, I.; Heeney, M.; Bailey, C.; Genevicius, K.; MacDonald, I.; Shkunov, M.; Sparrowe, D.; Tierney, S.; Wagner, R.; Zhang, W.; Chabinyc, M. L.; Kline, R. J.; McGehee, M. D.; Toney, M. F. *Nat. Mater.* **2006**, *5*, 328−333.
(26) Noriega, R.; Rivnay, J.; Vandewal, K.; Koch, F. P. V.; Stingelin, N.; Smith, P.; Toney, M. F.; Salleo, A. *Nat. Mater.* **2013**, *12*, 1038−1044.
(27) Yang, H.; Shin, T. J.; Yang, L.; Cho, K.; Ryu, C. Y.; Bao, Z. *Adv. Funct. Mater.* **2005**, *15*, 671−676.
(28) (a) Mei, J.; Bao, Z. *Chem. Mater.* **2013**, *26*, 604−615. (b) Fang, L.; Zhou, Y.; Yao, Y.-X.; Diao, Y.; Lee, W.-Y.; Appleton, A. L.; Allen, R.; Reinspach, J.; Mannsfeld, S. C. B.; Bao, Z. *Chem. Mater.* **2013**, *25*, 4874−4880. (c) Lei, T.; Wang, J.-Y.; Pei, J. *Chem. Mater.* **2013**, *26*, 594−603. (d) Lee, J.; Han, A. R.; Kim, J.; Kim, Y.; Oh, J. H.; Yang, C. *J. Am. Chem. Soc.* **2012**, *134*, 20713−20721.

## ■ NOTE ADDED AFTER ASAP PUBLICATION

Changes were made to Figure 2 and Table 1, and Figure S3 in the Supporting Information on October 14, 2014.